PCCP

PAPER

View Article Online
View Journal | View Issue

Cite this: *Phys. Chem. Chem. Phys.*, 2019, **21**, 5158

A new *ab initio* modeling scheme for the ion self-diffusion coefficient applied to the ε-Cu_3Sn phase of the Cu–Sn alloy†

Tom Ichibha, *[a] Genki Prayogo,[b] Kenta Hongo [cdef] and Ryo Maezono[af]

Received 8th October 2018,
Accepted 25th January 2019

DOI: 10.1039/c8cp06271d

rsc.li/pccp

We present a new scheme for modeling of the ion self-diffusion coefficient. Our scheme broadens the applicable scope of the '*ab initio* + modeling' approach, which combines modeling of the self-diffusion coefficient with *ab initio* predictions. Essential concepts in our scheme are 'domain division' and 'coarse-graining' of the diffusion network, according to calculated barrier energies. With the former concept, the diffusion network is divided into a few types of simple disjunct domains. Their networks are further simplified with the latter idea that groups some ion sites and regards them as just a single site. We applied this scheme to Cu diffusion in the ε-Cu_3Sn phase of the Cu–Sn alloy and succeeded in reproducing experimental diffusion coefficients in a wide range of temperature.

1 Introduction

Ion diffusion attracts broad interest from material researchers because it dominates various important phenomena in solids such as corrosion, monotectoid reactions, fracture, and degradation. In order to elucidate a microscopic mechanism of ion diffusion, *ab initio* calculation is one of the most powerful tools. For example, it can evaluate barrier energies of diffusion routes, with such techniques as the nudged elastic band (NEB) method.[1] Even also ion self-diffusion coefficients‡ have been reported theoretically[2–7] combining *ab initio* predictions with modeling schemes such as the five-frequency model.[8–10] However, these applications have been limited to just the simplest crystals, mainly due to the following reasons. First, systems appearing in practical situations often require a large size of the unit cell because of their long-range periodicity, which makes the calculation expensive, and often infeasible. This problem is especially severe, for example, when optimizing an ion path through a diffusion route using the NEB method, because it requires many force-field calculations for each of several transition structures. Second, it is always tough to take into account all of the ion diffusion processes, which is necessary to model the self-diffusion coefficient.

To overcome the difficulties, we introduce a couple of novel concepts in order to simplify the diffusion network. First, we classify the diffusion routes into three groups I–III, according to their barrier energies, $\Delta E_{\mathrm{I}} \ll \Delta E_{\mathrm{II}} \ll \Delta E_{\mathrm{III}}$. Since the barrier energy exponentially contributes to the diffusion coefficient (*i.e.* the Boltzmann factor), diffusion routes (III) can be excluded from the diffusion network. Then, the network may be divided into a few disjunct domains, and the expensive calculation for the large unit cell is replaced by cheaper calculations for these domains. This is the solution for the first difficulty. Second, the diffusion network in each domain is further simplified by coarse-graining: a vacancy moves almost freely through diffusion routes (I) compared with routes (II), so ion sites connected by routes (I) can be merged into just a single site. (We call it a representative site or rep-site.) Accordingly, the diffusion network falls into a coarse-grained one with the rep-sites, where it is much easier to model the self-diffusion coefficient by counting up possible diffusion processes.

Finally, we established a modeling scheme based on these concepts and applied it to obtain the Cu ion self-diffusion coefficient in the ε-Cu_3Sn phase of the Cu–Sn alloy. This system is an excellent example because it has long-range periodic structure and abundant experimental data of the self-diffusion

[a] *School of Information Science, JAIST, Asahidai 1-1, Nomi, Ishikawa, 923-1292, Japan. E-mail: ichibha@icloud.com; Tel: +81-8077049258*
[b] *School of Materials Science, JAIST, Asahidai 1-1, Nomi, Ishikawa, 923-1292, Japan*
[c] *Research Center for Advanced Computing Infrastructure, JAIST, Asahidai 1-1, Nomi, Ishikawa 923-1292, Japan*
[d] *Center for Materials Research by Information Integration, Research and Services Division of Materials Data and Integrated System, National Institute for Materials Science, Tsukuba 305-0047, Japan*
[e] *PRESTO, Japan Science and Technology Agency, 4-1-8 Honcho, Kawaguchi-shi, Saitama 322-0012, Japan*
[f] *Computational Engineering Applications Unit, RIKEN, 2-1 Hirosawa, Wako, Saitama 351-0198, Japan*

† Electronic supplementary information (ESI) available. See DOI: 10.1039/c8cp06271d

‡ When target ions are distributed nonuniformly in a crystal, their distribution changes macroscopically by thermal diffusion. This phenomena is called self-diffusion, and a measure of the speed is the self-diffusion coefficient.

coefficient is available.[11–16] The constructed model successfully reproduced the experiments in a wide range of temperature, better than a classical MD study by a digit.[17] Also we verified how well our modeling takes into account diffusion processes. It affects the accuracy of the evaluation of the correlation factor, which is a key quantity of modeling. We confirmed that the obtained correlation factor is quite reasonable, compared to a reference value of a two-dimensional hexagonal lattice.

In this section we briefly explained two essential concepts, 'domain division' and 'coarse-graining', for *ab initio* modeling of diffusion coefficients. They are described further with an example of Cu ion diffusion in ε-Cu_3Sn alloys and a brief explaination of how they are used to obtain the diffusion coefficients in Section 2. Detailed derivations of the formula are put in the ESI,† since they are too complicated and would make the main stream of the discussion unclear. The constructed model is carefully validated in Section 4 by comparing the self-diffusion coefficients with experimental values and, moreover, the correlation factor with the reference value. Finally, we summarize this work and review our scheme compared to the *ab initio* molecular dynamics method in Section 5.

2 Modeling

Domain division

The structure of the ε-Cu_3Sn phase is shown in Fig. 1a, which has long-range periodicity. In the previous interpretation, it consists of unit cells of Cu_3Ti-type structure with 1/2 shifts along the *a*-axis, every *M*/2 unit cell lining up along the *b*-axis.

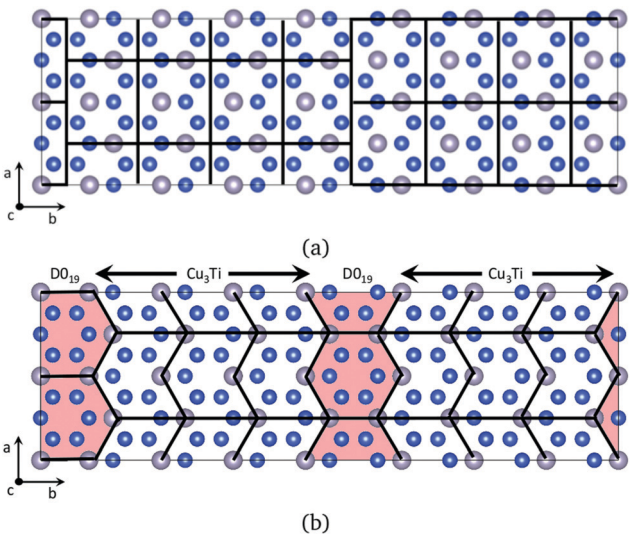

Fig. 1 A schematic picture of domain division for the ε-Cu_3Sn structure.[18] The blue balls represent Cu ions, and the gray balls Sn ions. Figure (a) shows the conventional interpretation for the long-range periodic structure. A Cu_3Ti-type unit cell (surrounded by a thick line) is shifted by 1/2 a period along the *a* direction in fractional coordinates, every *M*/2 (*M*: periodicity) unit cell lining up along the *b* direction. Figure (b) shows our new interpretation. (*M* − 2)/2 unit cells of Cu_3Ti-type structure and one $D0_{19}$-type unit cell appear periodically along the *b* direction. These pictures are made using VESTA.[19]

(*M* = 2, 4, 6, 8, and 12 have been reported experimentally.[18,20]) Our *ab initio* predictions revealed that ion jumps through diffusion routes passing between Sn sites hardly contribute to the self-diffusion because their barrier energies are much higher than the others by >30 kJ mol^{-1}. After excluding these routes, the network is divided into two types of simple domains, Cu_3Ti-type and $D0_{19}$-type, as shown in Fig. 1b. They exist in a ratio of (*M* − 2):2, so the self-diffusion coefficient is given as a weighted average of those with their existence ratio:

$$D_{\varepsilon\text{-}Cu_3Sn} = \frac{M-2}{M} D_{Cu_3Ti} + \frac{2}{M} D_{D0_{19}}. \quad (1)$$

Coarse-graining

Cu sites in the $D0_{19}$-type domain (Fig. 2) are positioned like hexagonal tubes composed of Cu sites surrounded by lines connecting Sn sites. Each tube consists of laminations of Cu ions arranged in a triangle shape, located in different *ab*-planes by 1/2 a period. (The hatched and the unhatched sites are on the different planes.) The barrier energy of route 3 is much higher than those of route 1 and 2 by >50 kJ mol^{-1}, so ions almost independently diffuse in each hexagonal tube. Also, route 1 has a much lower barrier energy than route 2 by >40 kJ mol^{-1}, so the vacancy much more easily moves in a triangle through route 1 than moving across two triangles through route 2. Therefore, the three sites forming the triangle are merged into just a single site (rep-site), which is named rep-site in the introduction. The diffusion network is coarse-grained into 1-dimensional ones along the *c*-axis composed of rep-sites as shown in Fig. 3. Since it is known that diffusion factors are zero in 1-dimensional lattices,[21]

$$D_{D0_{19}} = 0. \quad (2)$$

The diffusion network of the Cu_3Ti-type domain is also coarse-grained using the same analogy, yet into 2-dimensional

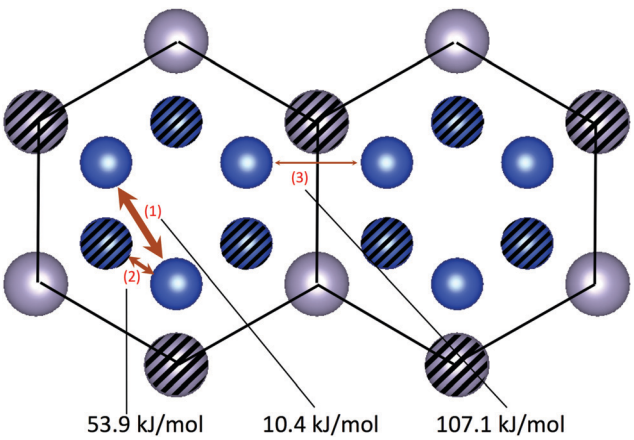

Fig. 2 Diffusion routes and barrier energies of Cu ions in the $D0_{19}$-type domain. The diffusion routes are shown as two-way arrows with their barrier energies. The blue balls represent Cu ions, and the gray balls Sn ions. The hatched balls are located on a *c* = 1/2 plane, and the unhatched ones are on a *c* = 0, 1 plane in fractional coordinates. Ion diffusion occurs in 1-dimensional tubes partitioned by the thick black lines because the energy barrier of route 3 across the thick lines is much higher than the others by >30 kJ mol^{-1}. This picture is made using VESTA.[19]

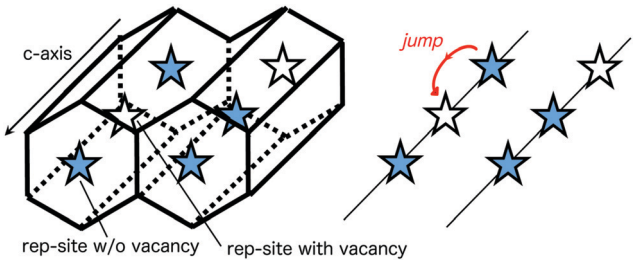

Fig. 3 A schematic picture of coarse-graining for the $D0_{19}$-type domain. The open and closed stars represent a rep-site including a vacancy and a fully occupied one. Since ions seldom jump perpendicular to the *c*-axis, the coarse-grained network is almost 1-dimensional.

ones: the barrier energies of route 6,6′ are much higher than the others by >30 kJ mol^{-1} so ion diffusion occurs in each layer partitioned by the thick zig-zag lines drawn in Fig. 4. Also, the barrier energies of route 3,3′ are much lower than the others by ~ 30 kJ mol^{-1}, so the three sites connected by route 3,3′ can be merged into a rep-site. After coarse-graining, the diffusion network falls into 2-dimensional ones including two types of diffusion routes *a* and $\tilde{c}$, as shown in Fig. 5. (Route *a* is parallel to the *a*-axis but route $\tilde{c}$ deviates from the *c*-axis.) In this case, the diffusion coefficient D_{Cu_3Ti} has a finite value.

Since the framework of 'coarse-graining' is based on the apparent differences in the barrier energies, one might worry about its general applicability when the barriers do not have such outstanding differences as in the present case. It is partly

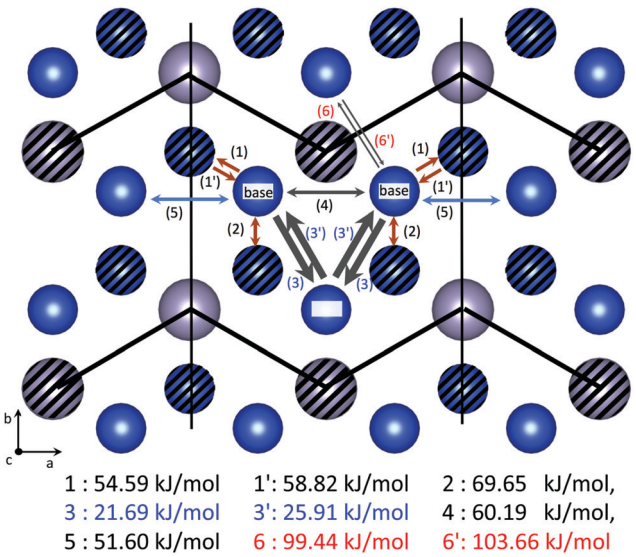

Fig. 4 Diffusion routes of Cu ions in the Cu_3Ti-type domain. The blue balls represent Cu ions, and the gray balls Sn ions. The hatched balls are located on a $c = 1/2$ plane, and the unhatched ones are on a $c = 0$, 1 plane in fractional coordinates. Three sites named top and bottom are merged into just a single site (rep-site). Diffusion routes connecting the adjacent rep-sites are shown as the red arrows (1,1′,2) and the blue ones (5), which are named route $\tilde{c}$ and *a* respectively. Barrier energies of every route are listed below the figure. The diffusion network is partitioned by the thick zig-zag lines, because route 6, 6′ has much higher energy barriers than the others by >30 kJ mol^{-1}. This picture is made using VESTA.[19]

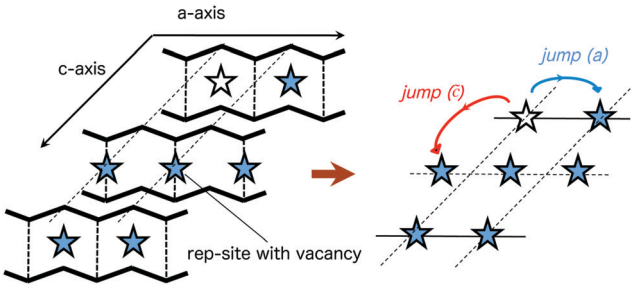

Fig. 5 A schematic picture of coarse-graining for the Cu_3Ti-type domain. The open and closed stars represent a rep-site including a vacancy and a fully occupied one. Since ions seldom jump in the perpendicular direction to the *ac*-plane, the coarse-grained network is almost 2-dimensional. The network contains two types of routes, *a* and $\tilde{c}$. Route *a* is parallel to the *a*-axis, and meanwhile, route $\tilde{c}$ is not parallel to the *c*-axis.

true that the applicability becomes limited, but it still works in the low temperature region: even with a smaller difference of the barrier energies like 1 kJ mol^{-1} compared to the case in Fig. 2 and 4, their Boltzmann factors differ by around ten times at 50 K. Meanwhile they surely become almost the same at 1000 K, and hence the coarse-graining is not working at the high temperature range. Not only due to this matter, but also due to other factors as explained in the last paragraph of section 'Results and Discussion', we note that the framework is generally reliable only in the lower temperature range.

Equations for the self-diffusion coefficient

From the consequences of the previous subsections, $D_{\varepsilon\text{-}Cu_3Sn}$ fully depends on D_{Cu_3Ti} as follows:

$$D_{\varepsilon\text{-}Cu_3Sn} = \frac{M-2}{M} D_{Cu_3Ti}. \quad (3)$$

The ε-Cu_3Sn phase is polycrystalline, where the grain boundaries face in different directions, so the ion diffusion in the phase should be isotropic. Thus, we evaluate D_{Cu_3Ti} as an average of diffusion coefficients over the entire angle:

$$D_{Cu_3Ti} = 1/3 \cdot (D(a) + D(c)). \quad (4)$$

Here, $D(a)$ $[D(c)]$ is the diffusion coefficient of Cu ions along the *a* (*c*)-axis in the Cu_3Ti-type structure.

The diffusion coefficient in a specific direction *w* (*e.g.* the *a* or *c*-axis) is given as

$$D(w) = \sum_j \frac{1}{2} D_j^* \cos^2 \theta_j(w). \quad (5)$$

Here, D_j^* is the contribution from ion jumps through route *j*. $\theta_j(w)$ is the angle between the ion jump and direction *w*. The projection of D_j^* is taken as squared $\cos\theta_j(w)$, because D_j^* has dimensions of squared length. The contribution D_j^* is given as the following equation:[21]

$$D^* = d^2 \cdot f \cdot C_v \cdot \eta \quad (6)$$

(index *j* omitted). *d* is the distance of the diffusion route. C_v is the vacancy formation rate given as a Boltzmann factor of the vacancy formation energy. η is the jump rate, given as a product

of a Boltzmann factor of the barrier energy and the vibration frequency. It is straightforward to calculate these quantities from *ab initio* calculations. Computational details and results are given in Section 3. Meanwhile, it is difficult to perform an analytical evaluation of the correlation factor f, which reflects the position exchanges sequentially occurring between the vacancy and the tracer ion: after an ion jump *via* the vacancy, the vacancy is at the back of the tracer. Thus, the vacancy tends to pull back the tracer at the first position exchange in the reverse direction of the ion jump. Moreover, following the first one, position exchanges can occur again and again, which always move the tracer in the reverse direction of the preceding tracer move. The correlation factor f represents how much the sequential exchanges affect the self-diffusion coefficient in total. Since the first exchange has the most significant contribution to the correlation factor, it must reduce D_j^* (*i.e.* $0 \leq f \leq 1$). It is tough to calculate this factor because we have to cover all of the vacancy tracks, which finally causes a position exchange between the vacancy and the tracer.

Now we return to the specific discussion on the Cu_3Ti-type structure, consisting of routes a and $\tilde{c}$. The contributions of ion jumps through both routes are denoted by $D_{a,\tilde{c}}^*$, respectively. According to eqn (5), the diffusion coefficients $D(a)$ and $D(c)$ are given as follows:

$$D(a) = D_a^* + 2D_{\tilde{c}}^* \cos^2 \theta_{a\tilde{c}}, \tag{7}$$

$$D(c) = 2D_{\tilde{c}}^* \cos^2 \theta_{c\tilde{c}} \tag{8}$$

In order to obtain $D_{a,\tilde{c}}^*$ from eqn (6), we will deduce the correlation factors $f_{a,\tilde{c}}$. They are formally given as[21]

$$f_{a,\tilde{c}} = 1 + 2\sum_{n'=1}^{\infty} \langle \cos\theta \rangle_{a,\tilde{c}}^{(n')}. \tag{9}$$

Here, $\langle \cos\theta \rangle_{a,\tilde{c}}^{(n')}$ is an n'th-order average cosine, which represents how much n' position exchanges between the vacancy and the tracer reduce the diffusion coefficient. The absolute value of $\langle \cos\theta \rangle_{a,\tilde{c}}^{(n')}$ gradually decreases with n' increasing, so we should sum up just finite numbers of terms until the average cosine converges to zero. However, even for the coarse-grained diffusion network, it is not straightforward to evaluate f because there are two kinds of diffusion routes a and $\tilde{c}$: it is different how the next position exchange occurs depending on whether the tracer moved through route a or $\tilde{c}$. Hence, we have to consider two patterns for every position exchange, so the number of patterns for n' exchanges increases in proportion to $2^{n'}$. This complexity prevents one from evaluating the correlation factor for the multiple types of diffusion routes that there are. We thought of a way to extend the theory established for the case in which there are multiple types of diffusion routes, by taking a simultaneous recurrence formula: (i) in the case of $n' = 1$, the average cosine is given as

$$\langle \cos\theta \rangle_{l=a,\tilde{c}}^{(l)} = \sum_k \frac{d_{L^{(l)}(k)}}{d_l} \cos\theta_k^{(l)} \cdot P_k^{(l)} \tag{10}$$

Here, $\frac{d_{L^{(l)}(k)}}{d_l} \cdot \cos\theta_k^{(l)}$ is the contribution of one position exchange between the tracer and the vacancy at site k. P_k is the probability that the position exchange occurs. $L^{(l)}(k)$ returns the type of route, a or $\tilde{c}$, used for the position exchange. (ii) In the case of $n' = n + 1$, $n + 1$ position exchanges means that n position exchanges occur after the first exchange through route a or $\tilde{c}$. On the other hand, the contribution of the first exchange is weakened by the nth order average cosine $\langle \cos\theta \rangle_{L^{(l)}(k)}^{(n)}$. The above explanation is expressed as the following recurrence formula:

$$\langle \cos\theta \rangle_{l=a,\tilde{c}}^{(n+1)} = \sum_k \frac{d_{L^{(l)}(k)}}{d_l} P_k^{(l)} \cdot \cos\theta_k^{(l)} \cdot \langle \cos\theta \rangle_{L^{(l)}(k)}^{(n)}. \tag{11}$$

In the ESI,† we provide detailed derivations to get $P_k^{(l)}$ by counting up the probabilities of the hopping accompanied by a bit of complicated mathematical manipulation. From the derived $P_k^{(l)}$, we have evaluated $\langle \cos\theta \rangle_{a,\tilde{c}}^{n'}$ *via* eqn (10) and (11), and hence the correlation factor $f_{a,\tilde{c}}$ *via* eqn (9). Then we can get the diffusion coefficient *via* eqn (3)–(8).

3 Computational details

We employed $2 \times 2 \times 2$ supercells for both Cu_3Ti-type and $D0_{19}$-type domains to reduce spurious interactions between two vacancies across the periodic boundaries. The lattice parameters are fixed at experimental values.[18] We used VASP[22] for the density functional calculation to evaluate the physical quantities. The barrier energies are evaluated with the climbing-nudged elastic band (c-NEB) method[1] implemented in VASP.[22] c-NEB needs the interpolated structures between both edges of the diffusion path as an input and optimizes them by connecting them by virtual 'springs'. c-NEB guarantees that one of the structures is exactly positioned at the saddle point of the potential surface finally, in which c-NEB is superior to the original NEB method.[23] We prepared 15 structures and set the spring coefficient as 5 eV $Å^{-2}$. We used the PBE functional[24] and PAW pseudopotentials provided in VASP[25] for all of the calculations. The DFT energies are converged to better than 0.5 kJ per unit cell with respect to k-point sampling and plane wave cutoff energy. The vacancy formation energy is given as $\Delta E_{vac} = E_{vac} - E_{perfect} + \mu_{Cu}$. Here, $E_{perfect}$ is the total energy of a perfect crystal and E_{vac} is that of a crystal including a vacancy defect. For the chemical potential of Cu ions, μ_{Cu}, we evaluated it as the total energy per atom of a face-centered Cu mono-crystal. All Cu sites are equivalent, and their vacancy formation energy is given as 16.60 kJ mol^{-1}. Meanwhile, the Cu_3Ti-type domain has two distinguishable Cu sites, 'top' and 'base', and their vacancy formation energies are calculated as $C_v^{(top)}$ = 25.94 kJ mol^{-1} and $C_v^{(base)}$ = 21.71 kJ mol^{-1}, respectively. We calculated the vibrational frequencies of tracer jumps with the harmonic approximation of the potential surface for ion jumps through every diffusion route: 1: 3.675×10^{12} s^{-1}, 1′: 3.575×10^{12} s^{-1}, 2: 4.152×10^{12} s^{-1}, 3: 3.155×10^{12} s^{-1}, 3′: 2.542×10^{12} s^{-1}, 4: 4.138×10^{12} s^{-1}, 5: 3.618×10^{12} s^{-1}.

(Vibrational frequencies of route 6 and 6′ are not calculated because they are already excluded from the diffusion network due to their high energy barriers.)

4 Results and discussion

Self-diffusion coefficient $D_{\varepsilon\text{-}Cu_3Sn}$ calculated by our model is compared with experimental and classical MD values in Fig. 6. Our results reproduce experimental values reasonably: the predicted values pass through just the middle of the experimental values. The different periodicities, $M = 4$ (a in Fig. 6) and $M = \infty$ (b in Fig. 6), give twice different values. Meanwhile, the scatter of the experimental values (c–h in Fig. 6) is much larger, and the experimental discrepancy cannot be explained by the differences of periodicity M. The previous classical MD[17] work (i in Fig. 6) overestimates our results and the average of experimental values by a digit, presumably due to using an empirical force-field. Another possible reason is that the time step used in the MD work is not small enough to evaluate the potential top of the diffusion route. (The time step is not shown in the MD paper.[17]) Nonetheless, this is unlikely to be true because the commonly used time step size is on the order of a few femtoseconds and it is much smaller than even the ion vibration frequencies shown in Section 3.

Fig. 7 shows the convergence of the correlation factors $f_{a,\tilde{c}}$ for the number of terms $n_{\max}$ to be summed in eqn (9). These graphs oscillate for small $n_{\max}$ because every position exchange somewhat counteracts the preceding tracer move: the first exchange counteracts the ion jump, and the second exchange similarly counteracts the ion move at the first exchange. Eventually, $f_{a,\tilde{c}}$ converge into constant values, and only they are needed to evaluate the model.

We verified the constructed model by confirming if the (converged) values of $f_{a,\tilde{c}}$ are reasonable by comparing them

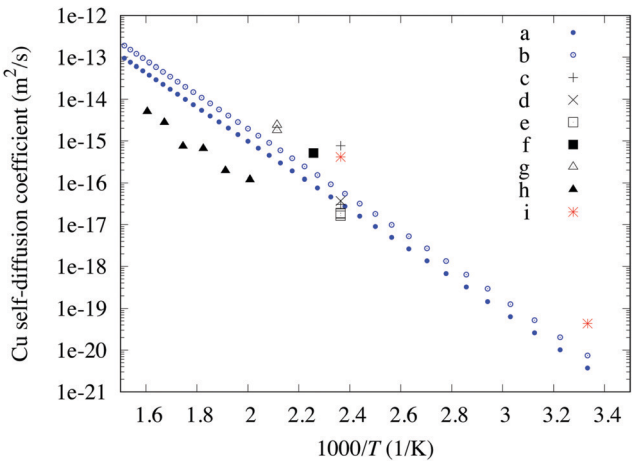

Fig. 6 This work [a: $M = 4$, b: $M = \infty$]; experimental values [c: B. Chao *et al.*,[11] d: B. Chao *et al.*,[12] e: Y. Yang *et al.*,[13] f: Y. Wang *et al.*,[14] g: S. Kumar *et al.*,[15] h: A. Paul *et al.*];[16] classical MD [i: F. Gao and J. Qu].[17] Comparison of the self-diffusion coefficient of Cu ions with an Arrhenius plot. The blue points represent our predictions with different periodicity M. The black and the red points represent the values reported from experiments and classical MD, respectively.

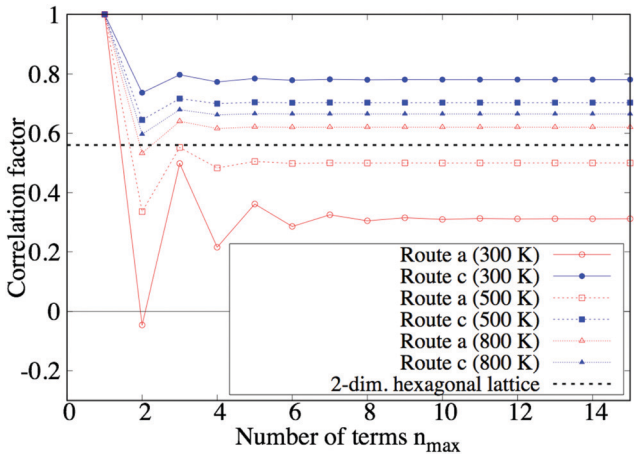

Fig. 7 Convergence of correlation factor $f_{a,\tilde{c}}$ at 300, 500, and 800 K. This figure shows how the correlation factor $f_{a,\tilde{c}}$ converges with the number of pull-backs to be counted up increasing. The black dotted line is the reference value of the correlation factor, which is calculated for a 2-dimensional hexagonal lattice, nearly equaling 0.56.[21]

with a reference value: if route a and $\tilde{c}$ were equivalent, the simplified diffusion network of the Cu_3Ti-type structure would be regarded as an almost ideal 2-dimensional hexagonal lattice (see Fig. 5). Thus, it is interesting to compare $f_{a,\tilde{c}}$ with the correlation factor of the lattice, ~ 0.56. First, in the case of low temperature ($T = 300$ K), f_a is lower and $f_{\tilde{c}}$ is higher than 0.56, respectively. This comes from the fact that vacancies move through route $l = a$ much more easily than through route $l = \tilde{c}$: the vacancy easily goes away from the tracer through route a after the tracer move ($l = \tilde{c}$), so position exchanges seldom happen, and $f_{\tilde{c}}$ becomes higher. On the other hand, for the tracer move $l = a$, the vacancy moves through route a along the same line many times, so position exchanges frequently happen and f_a becomes lower. In another way of thinking, the latter situation is similar to 1D diffusion so f_a becomes much lower. Second, in the case of high temperature ($T = 1000$ K), it is expected that both f_a and $f_{\tilde{c}}$ converge around 0.56 when the temperature increases. This is because routes a and $\tilde{c}$ are almost equivalent at high temperature, and the diffusion network is similar to an ideal 2D hexagonal lattice. The converged values are just 0.08 higher than 0.56. The small overestimation may be caused by the ignorance of vacancy tracks that include 3 routes or more. Nevertheless, the bias is quite small even at high temperature, compared to the dependence on periodicity M. Moreover, the bias is expected to get less at low temperature, because an infinite number of routes a is taken into consideration to count up vacancy tracks.

In addition to the reason we described at the end of the subsection, 'Coarse-graining', there are several other factors which would limit the applicability of the present framework within the low temperature range: in our scheme, we have taken into account only the 'barrier energies evaluated at zero temperature' as the dominating factor in the ionic diffusion. At finite temperature, other possible factors would arise such as the change in the barrier energies due to anisotropic

thermal expansion,[26] interactions between point defects, and anharmonic effects.[27] It is not practical to treat all these effects by extending the present *ab initio* based scheme. The present scheme would therefore be an appropriate approach within the low temperature range. Here we notice the complementary roles of the present strategy (for low temperature) and the MD-based one (high temperature). While the above 'thermal effects' could be captured well by the MD-based strategies, the slowing-down dynamics of the ionic jumps in the lower temperature range would be tough to capture by MD even with improved descriptions for longer time-scales such as the color-diffusion algorithm.[28,29]

5 Conclusions

We established a new modeling scheme to determine the ion self-diffusion coefficient, introducing some novel concepts. The scheme is applied to obtain the Cu self-diffusion coefficient in the ε-Cu_3Sn phase of the Cu–Sn alloy in this work. The highlights of our scheme are 'domain division' and 'coarse-graining' of the diffusion network, based on barrier energies predicted by *ab initio* calculations. In the former concept, the diffusion network is divided into several types of disjunct domains. Then, the calculation for the original large unit cell is replaced by those for the different types of simple domains, which significantly reduces the calculation cost. The diffusion network of our target system, ε-Cu_3Sn, is divided into two types of domains, which have 1- and 2-dimensional networks, respectively. In the latter concept, the diffusion networks of each domain are coarse-grained by merging some ion sites connected by routes having comparatively small energy barriers into just a single site (rep-site). This approximation is made on the grounds of the fact that the vacancy can move through these routes much more easily than through the others. As a result, it is established that the 1-dimensional domain never contributes to the self-diffusion[21] and counting up of vacancy tracks in the 2D domain is much simplified. Finally, the established model successfully reproduces experimental values, better than previous classical MD work by a digit.[17]

Conflicts of interest

There are no conflicts to declare.

Acknowledgements

The computation in this work has been performed using the facilities of the Research Center for Advanced Computing Infrastructure (RCACI) at JAIST. T. I. is grateful for financial suport from a Grant-in-Aid for JSPS Research Fellow (18J12653). K. H. is grateful for financial support from a KAKENHI grant (JP17K17762), a Grant-in-Aid for Scientific Research on Innovative Areas ''Mixed Anion'' project (JP16H06439) from MEXT, PRESTO (JPMJPR16NA) and the Materials research by the Information Integration Initiative (MI^2I) project of the Support Program for Starting Up Innovation Hub from Japan Science and Technology Agency (JST). R. M. is grateful for financial support from MEXT-KAKENHI (17H05478 and 16KK0097), from Toyota Motor Corporation, from I-O DATA Foundation, and from the Air Force Office of Scientific Research (AFOSR-AOARD/FA2386-17-1-4049). R. M. and K. H. are also grateful for financial support from MEXT-FLAGSHIP2020 (hp170269, hp170220).

Notes and references

1 G. Henkelman and H. Jónsson, *J. Chem. Phys.*, 2000, **113**, 9978–9985.
2 W. Qiong, L. Shu-Suo, M. Yue and G. Sheng-Kai, *Chin. Phys. B*, 2012, **21**, 109102.
3 M. Mantina, Y. Wang, L. Chen, Z. Liu and C. Wolverton, *Acta Mater.*, 2009, **57**, 4102–4108.
4 M. Mantina, S. L. Shang, Y. Wang, L. Q. Chen and Z. K. Liu, *Phys. Rev. B: Condens. Matter Mater. Phys.*, 2009, **80**, 184111.
5 S. Huang, D. L. Worthington, M. Asta, V. Ozolins, G. Ghosh and P. K. Liaw, *Acta Mater.*, 2010, **58**, 1982–1993.
6 S. Choudhury, L. Barnard, J. Tucker, T. Allen, B. Wirth, M. Asta and D. Morgan, *J. Nucl. Mater.*, 2011, **411**, 1–14.
7 X. Zhang, H. Deng, S. Xiao, Z. Zhang, J. Tang, L. Deng and W. Hu, *J. Alloys Compd.*, 2014, **588**, 163–169.
8 A. D. Leclaire and A. B. Lidiard, *Philos. Mag.*, 1956, **1**, 518–527.
9 M. Koiwa and S. Ishioka, *Philos. Mag. A*, 1983, **48**, 1–9.
10 M. Koiwa and S. Ishioka, *J. Stat. Phys.*, 1983, **30**, 477–485.
11 B. Chao, S.-H. Chae, X. Zhang, K.-H. Lu, M. Ding, J. Im and P. S. Ho, *J. Appl. Phys.*, 2006, **100**, 084909.
12 B. H.-L. Chao, X. Zhang, S.-H. Chae and P. S. Ho, *Microelectron. Reliab.*, 2009, **49**, 253–263.
13 Y. Yang, Y. Li, H. Lu, C. Yu and J. Chen, *Microelectron. Reliab.*, 2013, **53**, 327–333.
14 Y. Wang, S. H. Chae, J. Im and P. S. Ho, *2013 IEEE 63rd Electronic Components and Technology Conference*, 2013, pp. 1953–1958.
15 S. Kumar, C. A. Handwerker and M. A. Dayananda, *J. Phase Equilib. Diffus.*, 2011, **32**, 309–319.
16 A. Paul, C. Ghosh and W. J. Boettinger, *Metall. Mater. Trans. A*, 2011, **42**, 952–963.
17 F. Gao and J. Qu, *Mater. Lett.*, 2012, **73**, 92–94.
18 M. Van Sande, R. De Ridder, G. Van Tendeloo, J. Van Landuyt and S. Amelinckx, *Phys. Status Solidi A*, 1978, **48**, 383–394.
19 K. Momma and F. Izumi, *J. Appl. Crystallogr.*, 2011, **44**, 1272–1276.
20 X. Sang, K. Du and H. Ye, *J. Alloys Compd.*, 2009, **469**, 129–136.
21 H. Mehrer, *Diffusion in Solids: Fundamentals, Methods, Materials, Diffusion-Controlled Processes*, Springer, Berlin, Heidelberg, 2007.
22 G. Kresse and J. Furthmüller, *Phys. Rev. B: Condens. Matter Mater. Phys.*, 1996, **54**, 11169–11186.
23 H. Jónsson, G. Mills and K. W. Jacobsen, *Nudged elastic band method for finding minimum energy paths of transitions*, 1998, pp. 385–404.

24 J. P. Perdew, K. Burke and M. Ernzerhof, *Phys. Rev. Lett.*, 1996, **77**, 3865–3868.
25 G. Kresse and D. Joubert, *Phys. Rev. B: Condens. Matter Mater. Phys.*, 1999, **59**, 1758–1775.
26 M. Mantina, Y. Wang, R. Arroyave, L. Q. Chen, Z. K. Liu and C. Wolverton, *Phys. Rev. Lett.*, 2008, **100**, 215901.
27 T. Indoh and M. Aniya, *Phys. Res. Int.*, 2011, **2011**, 1–3.
28 P. C. Aeberhard, S. R. Williams, D. J. Evans, K. Refson and W. I. F. David, *Phys. Rev. Lett.*, 2012, **108**, 1–5.
29 J. O. Nilsson, O. Y. Vekilova, O. Hellman, J. Klarbring, S. I. Simak and N. V. Skorodumova, *Phys. Rev. B: Condens. Matter Mater. Phys.*, 2016, **93**, 1–7.